SCIENCE CHINA
Physics, Mechanics & Astronomy

•Article•

May 2024 Vol. 67 No. 5: 256111
https://doi.org/10.1007/s11433-023-2345-3

Correlating dynamic relaxation and viscoelasticity in metallic glasses

GuangHui Xing[1], Qi Hao[1], Fan Zhu[1], Yun-Jiang Wang[2,3], Yong Yang[4,5], Hidemi Kato[6], Eloi Pineda[7], Si Lan[8], and JiChao Qiao[1,9*]

[1] *School of Mechanics, Civil Engineering and Architecture, Northwestern Polytechnical University, Xi'an 710072, China;*
[2] *State Key Laboratory of Nonlinear Mechanics, Institute of Mechanics, Chinese Academy of Sciences, Beijing 100190, China;*
[3] *School of Engineering Science, University of Chinese Academy of Sciences, Beijing 100049, China;*
[4] *Department of Mechanical Engineering, College of Engineering, City University of Hong Kong, Hong Kong 999077, China;*
[5] *Department of Materials Science and Engineering, College of Engineering, City University of Hong Kong, Hong Kong 999077, China;*
[6] *Institute for Materials Research, Tohoku University, Sendai 980-8577, Japan;*
[7] *Department of Physics, Institute of Energy Technologies, Universitat Politècnica de Catalunya, Barcelona 08019, Spain;*
[8] *School of Material Science and Engineering, Herbert Gleiter Institute of Nanoscience, Nanjing University of Science and Technology, Nanjing 210094, China;*
[9] *State Key Laboratory of Clean and Efficient Turbomachinery Power Equipment, Northwestern Polytechnical University, Xi'an 710072, China*

Received November 20, 2023; accepted February 6, 2024; published online April 11, 2024

Relaxation dynamics, essential for the structural evolution of non-equilibrium systems like glassy materials, remain enigmatic. Here, we explore relaxation dynamics and viscoelastic properties in three types of metallic glasses with distinct β relaxation behavior. In systems with significant β relaxation, stress relaxation and creep experiments reveal a transition from two-step to one-step relaxation with rising temperature. However, such a phenomenon is absent in systems with weaker β relaxation. We model the two-step relaxation process using a double Kohlrausch-Williams-Watts equation, and the obtained relaxation times elegantly adhere to the Arrhenius relationship. By combining fitted activation energies with theoretical analysis, we conclusively attribute these relaxation processes to β relaxation and α relaxation, respectively. Finally, we analyze the relaxation time spectra of two processes and establish a comprehensive picture linking dynamic relaxation with viscoelasticity. Our study provides new strategies for probing the complex relaxation behaviors of glasses from the perspective of viscoelasticity.

metallic glasses, dynamics relaxation, two-step relaxation, stress relaxation, creep

PACS number(s): 61.43.Dq, 62.40.+i, 62.20.Hg

Citation: G. H. Xing, Q. Hao, F. Zhu, Y.-J. Wang, Y. Yang, H. Kato, E. Pineda, S. Lan, and J. C. Qiao, Correlating dynamic relaxation and viscoelasticity in metallic glasses, Sci. China-Phys. Mech. Astron. **67**, 256111 (2024), https://doi.org/10.1007/s11433-023-2345-3

1 Introduction

Glass, an amorphous solid, is typically formed by rapidly cooling a supercooled liquid below its glass transition temperature (T_g), leading to a non-equilibrium energy state that manifests an intricate relaxation spectrum across a wide range of temperatures and timescales [1-10]. Relaxation dynamics plays a pivotal role in determining the characteristics and potential applications of amorphous materials [9], but understanding this complex phenomenon is one of the most intricate issues in materials science and condensed matter physics [1,6,8,9,11]. When cooling most glass-form-

*Corresponding author (email: qjczy@nwpu.edu.cn)

ing melts, the single relaxation process that occurs at elevated temperatures becomes decoupled into distinct α and β relaxation modes [1,2,6,12,13]. Above T_g, α relaxation serves as the dominant relaxation in liquids [2,9] and it is intimately tied to viscous flow and the glass transition, reflecting large-scale atomic restructuring [1,2,14,15]. As the temperature falls below T_g, the atomic mobility decreases, resulting in the freezing of α relaxation [1,2]. Thenceforth, Johari-Goldstein relaxation or β relaxation, characterized by a local motion in loosely packed isolated regions [9] and a restricted dynamic nature [16], controls the evolution of nanoscale heterogeneity [17] and structural relaxation [18,19].

In the realm of physical aging and the glass transition, the roles of α and β relaxations have been identified [17,20-24]. This naturally prompts the question: How does dynamic relaxation manifest during deformation processes? Numerous theoretical investigations have been conducted on the viscoelastic response of metallic glasses (MGs) when subjected to mechanical stimuli, employing various theoretical frameworks such as the free volume [25], shear transition zone [26], quasi-point defects [27], cooperative shear model (CSM) [28], flow units model [29] among others. However, few models have directly connected dynamic relaxation with viscoelasticity, which hampers the understanding of the underlying microscopic mechanisms. According to the CSM, the β relaxation is associated with isolated flow units within an elastic matrix, while the α relaxation is related to atomic infiltration, which leads to the collapse of the enclosed matrix and elastic breakdown [28,30]. Based on this background, a physical depiction of deformation in MGs connected with the potential energy landscape was developed [31]. The equivalence of the activation energy of β relaxation and the potential-energy barrier of STZs demonstrated that they share a common microstructural origin [32]. The flow units model established inherent correlations among the development of flow units, β relaxation, deformations, relaxation maps, and the energy landscape [33]. Additionally, the comparable stretched exponential behavior of the α relaxation and stress relaxation indirectly corroborates the potential relationship between viscoelasticity and dynamic relaxation [9,34]. Our previous research has identified two intriguing manifestations of β relaxation in stress relaxation [35,36].

Dynamic mechanical analysis under small deformation perturbations can effectively discern the multi-stage dynamic relaxation processes in MGs [9,37-39]. However, in conventional static viscoelastic deformations such as stress relaxation and creep, the influence of multi-stage relaxation has not been observed. This limitation stems from the precision and sampling rate constraints of current viscoelastic testing instruments, which hinder an accurate experimental resolution at short time scales. In this context, two significant questions need to be addressed: Understanding the role of dynamic relaxation in viscoelasticity, probing α relaxation below T_g in the glassy state, and assessing the impact of β relaxation on the mechanical response.

In this article, we analyzed the relaxation dynamics of viscoelastic deformation by combining dynamic mechanical analysis with creep and stress relaxation experiments. We selected three types of metallic MGs with different behaviors of β relaxation and conducted experiments from room temperature to temperatures above the β relaxation. Our research reveals that the type of β relaxation significantly impacts the viscoelastic deformation. In systems characterized by distinct β peaks, the single-step relaxation process observed at high temperatures during static viscoelastic deformation undergoes a transition towards a two-step relaxation process at low temperatures. This transition is believed to be due to the decoupling between β and α relaxation timescales. This significant finding not only provides new insights into relaxation behavior in glassy systems but also establishes a direct link between complex relaxation behavior and static viscoelastic deformation.

2 Materials and methods

2.1 Sample preparation

The $La_{20}Ce_{20}Y_{20}Ni_{20}Al_{20}$ (labeled as La_1-MG) [40], $La_{30}Ce_{30}Ni_{10}Al_{20}Co_{10}$ (La_2-MG) [40], $La_{60}Ni_{15}Al_{25}$ (La_3-MG) [41], $Pd_{42.5}Ni_{30}Cu_{7.5}P_{20}$ (Pd-MG) [42] and $Zr_{50}Cu_{34}Ag_8Al_8$ (Zr-MG) [43] were selected as the model alloys. To produce the metallic glass ribbons, pure metals with a purity greater than 99.99% were arc-melted in an argon atmosphere to create master alloys. The melting process was repeated six times to ensure the ingots were chemically homogeneous. Finally, a single-roller melt-spinning technique was used under an argon atmosphere to produce metallic glass ribbons approximately 35 μm thick.

2.2 Mechanical tests

2.2.1 Dynamic mechanical analysis

A commercial dynamic mechanical analyzer (DMA, TA 850) was used to characterize the dynamic mechanical relaxation processes of the MGs. During the DMA experiments, a sinusoidal stress was applied to the samples, and the corresponding strain was measured. The storage modulus E', the loss modulus E'', and the loss factor $\tan\delta = \frac{E''}{E'}$ were determined. The DMA experiments of the MGs were conducted in a tensile mode with a heating rate of 3 K/min and driving frequencies of 1, 2, 4, and 8 Hz, as shown in Figure S1 in the Supplementary Information.

2.2.2 Stress relaxation and creep

Tensile stress relaxation and creep measurements were carried out on ribbon samples using a TA Q850 DMA. The tests were conducted over a consecutive range of temperatures, from room temperature to the peak temperature of β relaxation T_β. For the stress relaxation experiment, a constant strain of 0.4% was rapidly applied to the sample and held for 30 min to record the stress decay. In the creep experiment, a constant force of 4 N was applied, and the strain was recorded as a function of time. To minimize the effects of thermal fluctuations, clamp thermal expansion, and ribbon recovery, a 30-min stabilization period was implemented after each temperature change. Additionally, to ensure the accuracy of the strain value, the length of the sample was measured before and after each test. Additional tests with different strain and force values were also performed. Further experimental details are presented in the Supplementary Information.

3 Results

3.1 Mechanical spectrum and viscoelastic deformation

Figure 1(a)-(c) illustrate the temperature dependence of the normalized loss modulus $E''/E''_{\max}$ determined by DMA. At a driving frequency of 1 Hz, the maximum loss modulus $E''_{\max}$, which corresponds to the α relaxation peak, is observed at T_α = 508, 585, and 719 K for the La_1-MG, Pd-MG, and Zr-MG, respectively. The β relaxation is evident as a distinct peak for the La_1-MG, a shoulder for the Pd-MG, and an excess wing that is merged into the α relaxation for the Zr-MG. The β relaxation is considered a reversible process of atomic rearrangement in localized flow units, and a significant β relaxation peak indicates that nanoscale localized flow behavior occurs below the T_g [33]. In order to separate the contribution of β and α relaxation in the temperature spectrum, methods detailed in Supplementary Information were used to fit the curves in Figure 1(a)-(c). The fitting of the β relaxation is depicted by the blue region, whereas the red region represents the contribution of the α relaxation. The yellow gap area between the α and β peaks implies the occurrence of cooperative interactions.

MGs with different β relaxation behaviors also exhibit different static viscoelastic properties. Figure 1(d)-(f) depict the isothermal stress relaxation spectra of La_1-MGs, Pd-MG and Zr-MG obtained at increasing temperatures from room temperature to 355, 500 and 510 K, respectively. The stress $\sigma(t)$ is normalized by its initial value at t = 0. La_1-MGs display a significant two-step decay process in their stress relaxation curves, characterized by a shoulder transition in the 1-100 s region that becomes more pronounced at lower temperatures, indicating a decoupling of the relaxation process in the glass state below T_β. In contrast, Pd-MG and Zr-MG exhibit a single relaxation process over a broad temperature range. The observed phenomenon of decoupling relaxation in the stress relaxation tests, which is present in all three La-MGs with significant β relaxation peak (Figure S2), indicates a close relationship between this phenomenon and the degree of separation between β relaxation and α relaxation in the dynamic mechanical spectrum.

The stress relaxation spectra manifested in La-based MGs bear a remarkable resemblance to the relaxation spectra observed in density fluctuations in Lennard-Jones glasses [44], colloidal suspensions [45], and molecular supercooled liquids [46]. At high temperatures, the relaxation dynamics exhibit a simple exponential decay, while at lower temperatures, a two-stage decay behavior emerges. Consistently with the predictions of the mode-coupling theory (MCT) for the intermediate scattering function in liquids [15,47], the initial rapid process, usually described by a single exponential decay, is attributed to restricted displacements of particles in the local environment due to the cage effect, while the subsequent slow process is characterized by a stretching exponent decay. However, our study focuses on stress relaxation in a completely different temperature range in the deep nonequilibrium glassy state. The relaxation decoupling phenomenon observed in Figure 1 appears to be closely related to the presence of the β, Johari-Goldstein type relaxation and differs from the physical origin of the fast β relaxation in MCT.

Similar phenomena can also be observed in another type of viscoelastic deformation test. Figure 1(g)-(i) show the creep curves of three different MGs in a logarithmic time scale. All La-MGs with significant β relaxation exhibit a clear separation of the creep process, as observed in the inset of the normalized strain curves (Figure S2). The normalized strain evolves from an evident shoulder-like behavior at low temperatures to a concave function at high temperatures. In contrast, the Zr-MG normalized strain curves collapse onto a Kohlrausch-Williams-Watts (KWW) function for all the temperatures, as shown by the black curve in the illustration, demonstrating its time-temperature equivalence. Notably, the Pd-MG exhibits a transition over temperature from a single-step to a two-step relaxation of the normalized creep curves. This can be attributed to the partial separation of α and β relaxation in the dynamic relaxation spectra, which is not discernible in stress relaxation but becomes visible in creep.

3.2 Model for mechanical relaxation

The glass relaxation behaviors are generally found to follow a KWW function [48]:

$$f(t) = \exp[-(t/\tau)^{\beta_{\mathrm{KWW}}}], \quad (1)$$

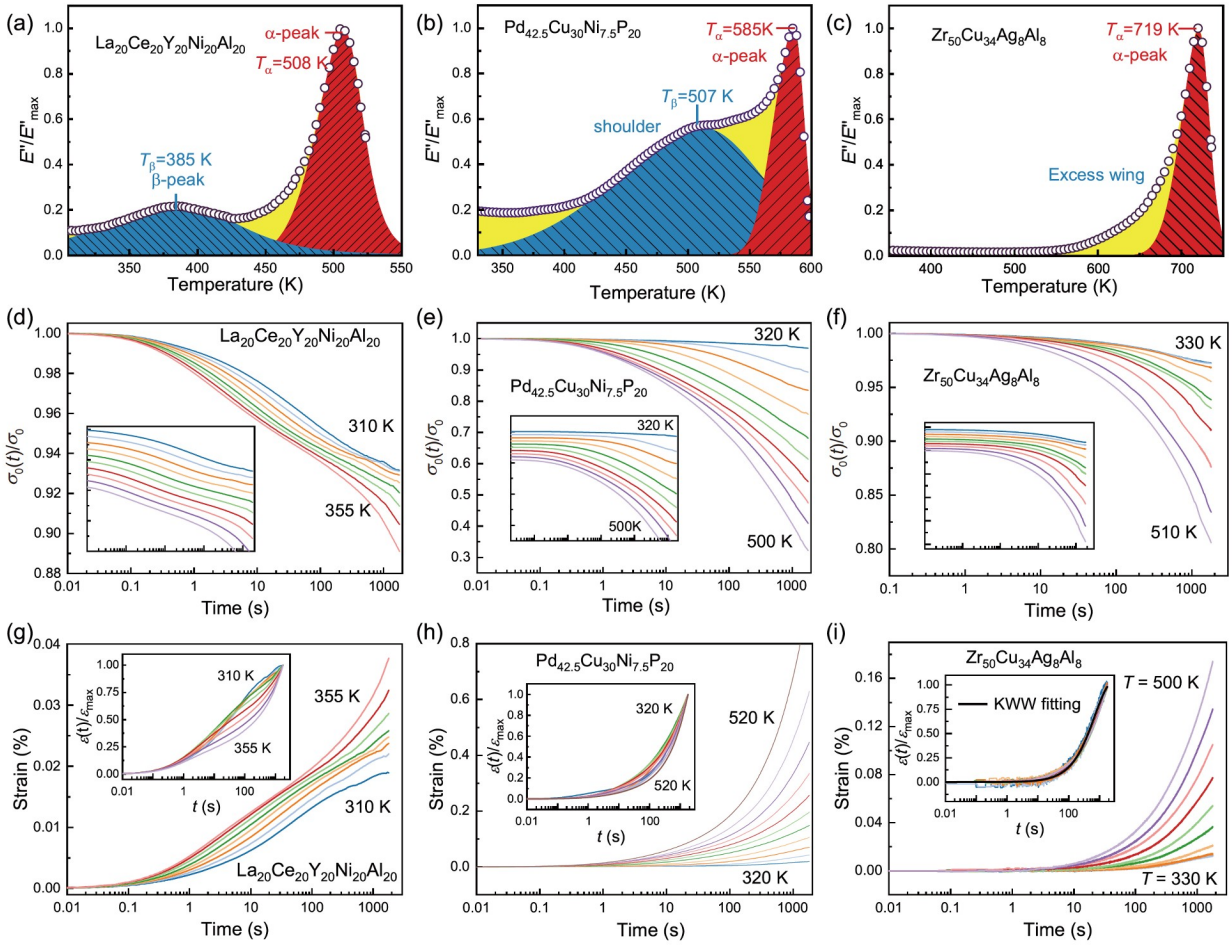

Figure 1 (Color online) The dynamic relaxation spectra and deformation behaviors of three prototypical MGs with different β relaxation features, namely $La_{20}Ce_{20}Y_{20}Ni_{20}Al_{20}$, $Pd_{42.5}Cu_{30}Ni_{7.5}P_{20}$ and $Zr_{50}Cu_{34}Ag_8Al_8$. From left to right, the panels correspond to the respective three MGs. Panels (a)-(c) show the normalized loss modulus E''/E''_{max}, where the blue region and the red region correspond to the KWW fitting of the β relaxation and the α relaxation process, respectively, and the yellow region is the cooperative interaction area and other processes. Panels (d)-(f) illustrate the normalized stress relaxation curves, with the corresponding semi-log plot shown in the insets. Panels (g)-(i) depict the creep strain evolution at different temperatures, with the inset showing the normalized strain.

where τ is the relaxation time and β_{KWW} a dimensionless stretched exponent satisfying $0 < \beta_{KWW} < 1$, the case $\beta_{KWW} = 1$ corresponds to a simple exponential decay.

For the two-step relaxation processes mentioned earlier, a single-KWW equation does not work. Therefore, we adopted a double KWW function as the fitting model [5], which assumes that both relaxation processes are described by stretch exponentials:

$$\sigma(t)/\sigma_0 = A\exp\left[-(t/\tau_{slow})^{\beta_{slow}}\right] + (1-A)\exp\left[-(t/\tau_{fast})^{\beta_{fast}}\right], \quad (2)$$

$$\varepsilon(t)/\varepsilon_0 = A\left\{1-\exp\left[-(t/\tau_{slow})^{\beta_{slow}}\right]\right\} + (1-A)\left\{1-\exp\left[-(t/\tau_{fast})^{\beta_{fast}}\right]\right\}, \quad (3)$$

where A is the strength of slow relaxation process, τ_{slow} and τ_{fast} are the relaxation times of the slow and fast relaxation process, respectively, β_{slow} and β_{fast} are the stretched exponents, σ_0 is the initial stress from experimental data, and ε_0 is the strength of anelastic strain obtained from the fitting. Eq. (2) is utilized to fit stress relaxation curves, while eq. (3) is employed to fit creep data. Fitting details are given in Figure S3.

3.3 Relation between dynamic and mechanical relaxations

As shown in the inset of Figure 2(a) for a KWW relaxation process, the relaxation time τ is the minimum of the rate of change function, and β_{KWW} represents the degree of stretch of the curve. Therefore, we can identify the fast relaxation and determine its relaxation time by analyzing the behavior of $d\sigma/d\ln(t)$. This method reduces the number of fitting parameters and makes the fitting results more accurate. Figure 2(a) illustrates the evolution of La_1-MG's fast re-

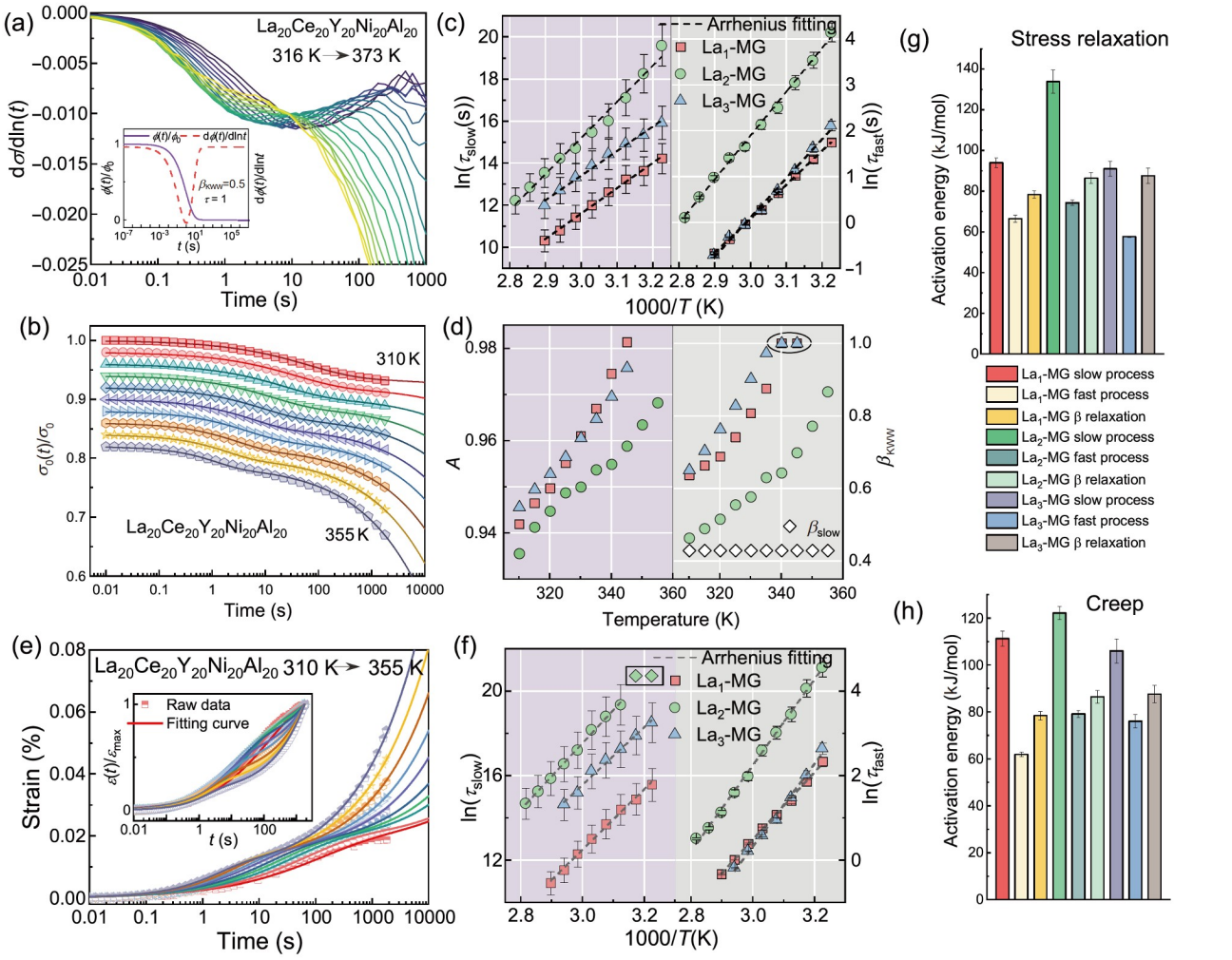

Figure 2 (Color online) Two-step relaxation phenomenon in stress relaxation and creep. (a) The temporal evolution of the logarithmic derivative of stress with respect to time, $d\sigma/d\ln(t)$, at different temperatures. The presence of a valley on the curve indicates the existence of a relaxation time. Inset shows the characteristics of individual KWW functions and the time evolution of $d\sigma/d\ln(t)$, where $\beta_{KWW} = 0.5$, $\tau = 1$. (b) Experimental data and fitting curves using eq. (2) for stress relaxation below the β relaxation temperature. (c) The logarithm of the two relaxation times (τ_{slow} and τ_{fast}) as a function of temperature for the three La-based MGs, where the black dashed lines represent the best fit to τ. (d) The temperature dependence of the fitting parameters A and β_{KWW} in eq. (2). (e) The creep data (scatter plot) of the La_1-MG at different temperatures, along with the fitting curve (solid line) according to eq. (3). Inset shows the normalized strain. (f) Arrhenius plot of the relaxation times τ_{slow} and τ_{fast}. The diamond-shaped green points in the black box indicate the divergent data. (g) Activation energies of two distinct processes obtained by stress relaxation in the three systems. (h) The activation energies of fast and slow relaxation processes. The error bars denote fitting uncertainty.

laxation with temperature, transitioning from a distinct valley at low temperatures to a shoulder-like pattern at higher temperatures. Notably, for curves with shoulder features, direct extraction of relaxation time is not feasible. Instead, parameters need to be obtained by fitting the corresponding stress relaxation curve, which can affect the reliability of the result. To maintain precision, our study focuses solely on the temperature range where significant fast relaxation occurs, typically around 20 K below the peak temperature of β relaxation T_β. It is commonly accepted that the stretched exponent β_{KWW} reveals the heterogeneous characteristics of structural relaxation dynamics [49,50]. Experimental measurements and molecular dynamics simulations in gorilla glass and MGs have demonstrated a stretched exponential decay with $\beta_{KWW} = 3/7$ at room temperature [48,51,52]. We adopt this value for the slow relaxation when the experimental time window does not permit a proper characterization of the slow component.

Based on the constraints on the fitting parameters mentioned above, we obtain a good fit for the stress relaxation data, as shown in Figure 2(b) and Figure S6. The evolution of the fitting relaxation times with $1000/T$ for stress relaxation of three La-based MGs is shown in Figure 2(c). All three La-based MGs exhibit a separation of fast and slow relaxation processes, where the relaxation time of the fast process is between 1-100 s, and that of the slow process is between

10^5-10^9 s. Both $\ln\tau_{fast}$ and $\ln\tau_{slow}$ exhibit significant linear relationships with the inverse temperature. As shown in Figure 2(g), the activation energies of the fast relaxation process for the three La-based MGs are obtained through Arrhenius fitting and are found to be 66.47, 74.26 and 57.66 kJ/mol, which is close to the activation energy of β relaxation obtained from DMA (as supported by Figure S7). The activation energies of the slow relaxation process were found to be 93.97, 91.01 and 133.87 kJ/mol, respectively. Surprisingly, their values are smaller than the activation energy of the α relaxation process obtained by the DMA technique [7,9,53], as will be analyzed in detail in the discussion section.

The fitting parameters A and the stretching exponent β_{KWW} are presented in Figure 2(d). At room temperature, fast relaxation accounts for only about 6% of the entire process. As the temperature increases, the proportion of the slow relaxation process in the entire relaxation gradually increases until the fast process is no longer distinguishable at a certain temperature, resulting in a transition from two-step relaxation to single-step relaxation. The white diamond symbols in the right part of Figure 2(d) represent the fixed parameter β_{slow} = 3/7, while β_{fast} shows an increasing trend with increasing temperature. It is noteworthy that in the La_1-MG and La_3-MG, the parameter β_{fast} quickly reaches the upper limit of 1. The upper limit is set artificially because the stretching exponent relaxation will turn into a "compression" exponent when $\beta_{KWW} > 1$. This anomalous compression decay has been observed in the microscopic dynamics of various systems, including soft matter [54], colloidal glasses [45], and MGs [5,55-57], and is attributed to ballistic particle motion driven by randomly distributed local stress dipoles [56]. Normally, the compressed relaxation process is weakly influenced by temperature, with activation energy below 0.1 eV, indicating the dominance of local stress [5,55-57]. However, the fast relaxation observed in this work exhibits a higher activation energy and is more influenced by temperature. Consequently, it is proposed that this relaxation process undergoes a transition from stretching exponential relaxation to simple Debye relaxation as temperature increases rather than becomes a compressed exponential relaxation.

Pioneering work found that creep deformation in MGs is mainly composed of viscoelastic and viscoplastic relaxation [58-60]. At low temperatures, the viscoelastic relaxation strength during creep is linearly proportional to the applied stress and is fully recoverable upon unloading [59]. In this study, creep was conducted between room temperature and the T_β for 1800 s, with a very small viscoplastic strain component, allowing eq. (3) with an upper deformation limit to accurately fit the data and effectively distinguish the two relaxation processes. The creep experiment results of La_1-MG and the fitting results are shown in Figure 2(e) and Figure S8, where the fitting curve shows a nice fit and a transition from fast relaxation to slow relaxation. As the temperature increases, the fast relaxation process gradually weakens. The fitted relaxation time shows an Arrhenius relationship with temperature, similar to stress relaxation. The stretching exponent β_{KWW} and relaxation strength A are also consistent with the stress relaxation results. It is worth noting that the green diamond points inside the black box in Figure 2(f) exhibit a relaxation time that reaches the upper limit of the fitting range. This is because the experimental temperature is much lower than the β relaxation, and the curve shows a transition plateau at 1800 s. In this case, during the experimental time, only the fast relaxation process was reached, resulting in the different fitting result of the slow relaxation process. This also demonstrates the perfect decoupling of the two-step relaxation process during creep deformation. The activation energies obtained from the Arrhenius fitting are shown in Figure 2(h). For the fast process are 61.87, 79.17, 76.05 kJ/mol and for the slow process are 111.19, 122.10, 105.97 kJ/mol. These values are totally comparable with the ones obtained in the stress relaxation tests.

To gain a deeper understanding of the two-step relaxation process during stress relaxation and creep in La-based MGs, we conducted stress relaxation experiments at different strains and creep experiments under various loads. Remarkably, all tests remained within the elastic range. As shown in Figure 3(a) and (f), the two sets of curves largely overlap after normalizing all curves. The double KWW function fitting parameters for stress relaxation experiments are presented in Figure 3(b) and (c), with all parameters being fairly similar when the strain is below 0.8%, indicating that our chosen experimental parameters were within the linear elastic regime. The initial stresses obtained at different strains also exhibit consistent characteristics. The evolution of $d\sigma/d\ln(t)$ demonstrates that the transition from fast relaxation to slow relaxation became faster when increasing strain above 0.8%, which indicates the sensitivity of the rapid relaxation processes to viscoelastic deformation. The fitting results of creep curves under different loads also show that the experimental parameters of 4 N remain within the linear viscoelastic range. We also conducted creep experiments under different temperatures and loads of 2, 4, 6, and 8 N to obtain the activation energy changes of the fast relaxation process, as shown in Figure 3(h). The specific experimental results are shown in Figure S10. We found that the activation energy of the fast process slightly increases with increasing load, which seems to contradict our understanding of thermal activation. This study proposes that larger forces can activate more micro-defects, while creep deformation under smaller loads excites fewer atomic movements. Even with more stress activation assistance, creep deformation under larger loads still requires more thermal energy to excite atomic movements in response to its macroscopic deformation.

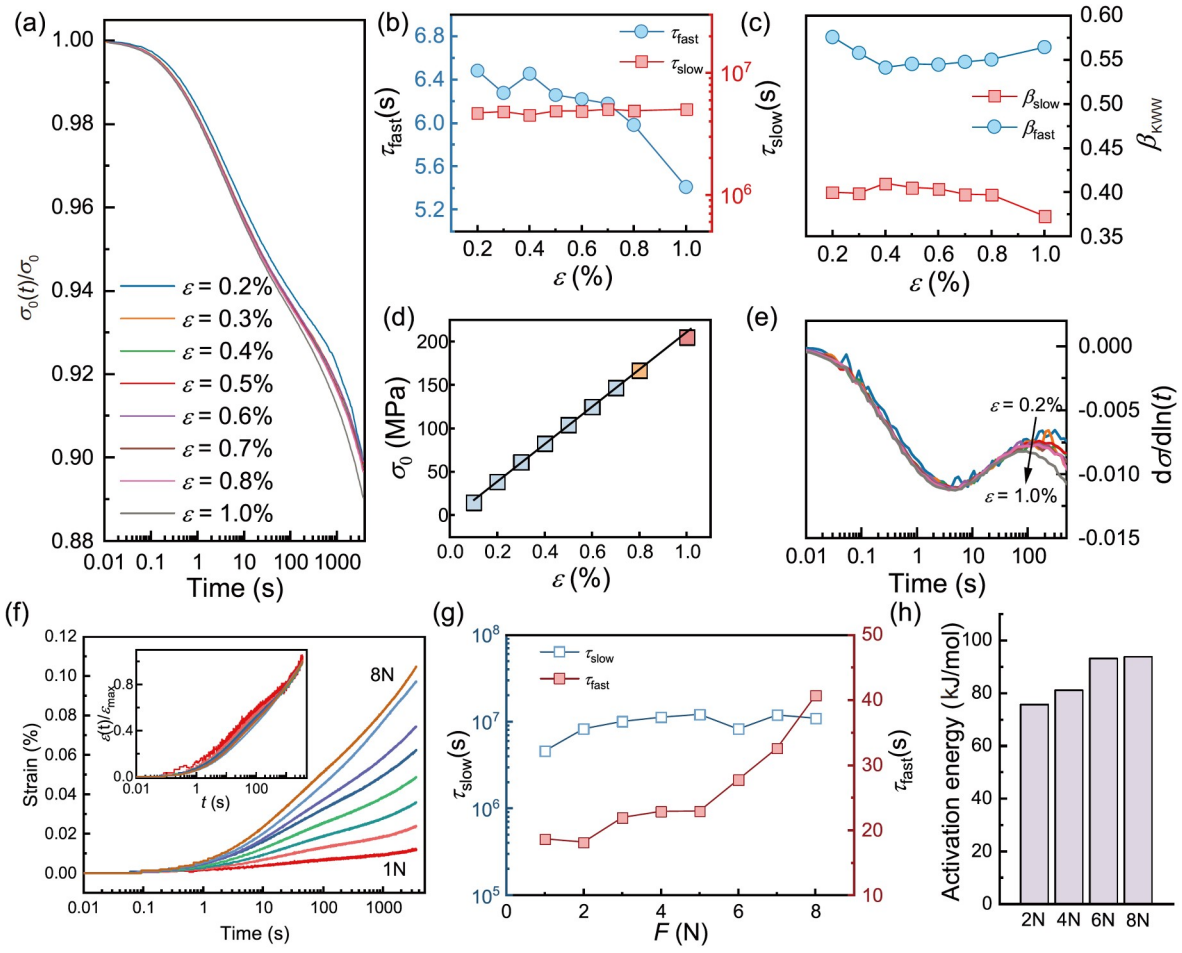

Figure 3 (Color online) (a) Stress relaxation profiles of the La_1-MG at 335 K with different initial strains, fitted with eq. (2). (b), (c) display the dependence of the relaxation time and stretched exponent versus strain, respectively. (d) The initial stress σ_0 as a function of strain. (e) The temporal evolution of dσ/dln(t) under varying strains. (f) The creep curves of the La_1-MG under different stresses, with the normalized strains in the inset, for better comparison of the relaxation time variations. (g) Relaxation times are for fast and slow processes. (h) Comparison of the activation energies for the fast relaxation process under 2, 4, 6, 8 N.

4 Discussion

As mentioned earlier, it is essential to discuss the physical mechanisms underlying the two-step relaxation process during the viscoelastic deformation of MGs. In other two-step relaxation studies, Luo et al. [5] attributed the fast relaxation to ballistic motion facilitated by local stress at the atomic scale, while the slow relaxation corresponds to larger-scale and more dynamic atomic structural rearrangement. The dynamics of the glass-forming liquid $Ca_{0.4}K_{0.6}(NO_3)_{1.4}$ [61] were interpreted in line with the MCT [14,15,47], suggesting that the fast relaxation is related to cage dynamics in glasses, while the slow relaxation is related to α relaxation. Yuan et al. [62] found that the fast relaxation is caused by local segmental motion of the surface, while the slow relaxation is the result of internal body segmental dynamics. In our study, we found a close relationship between fast relaxation and β relaxation. First, the two-step relaxation process only exists in systems with a significant separation between the β and α relaxation, while Zr-based MGs with an excess wing exhibit only a single stretched relaxation process. Second, relaxation decoupling in viscoelastic deformation occurs at temperatures of 10-20 K below but close to the T_β. Third, the fast relaxation observed in viscoelastic deformation in La-based MGs has an activation energy extremely close to β relaxation as determined by DMA. Figure 4 shows the relaxation time calculated from DMA, creep, and stress relaxation curves in La_1-MG. Aligning and overlaying the two fast relaxation times τ_{fast} with the β relaxation times τ_β, all relaxation times overlap essentially, demonstrating their common physical origin. Hence, it is reasonable to attribute the fast relaxation to β relaxation.

Identifying the physical origin of the slow process in creep and stress relaxation is challenging because the calculated activation energy does not match with any expected relaxation processes. α relaxation is typically frozen below T_g in glasses and cannot be detected within the frequency range of DMA [2,9]. According to the Tool-Narayanaswamy-Moy-

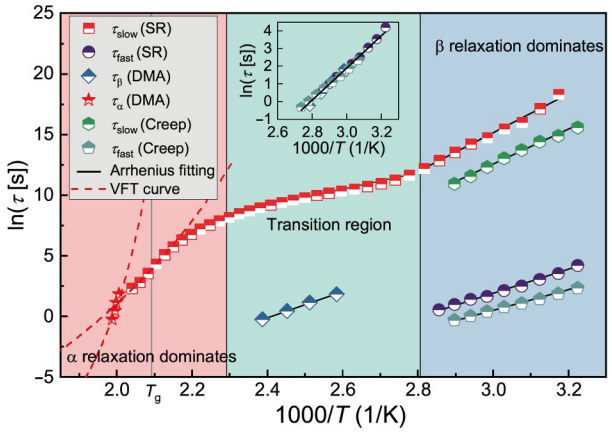

Figure 4 (Color online) The relaxation map of the La_1-MG. The plot shows α relaxation and β relaxation times determined from DMA (τ_β and τ_α), alongside the fast and slow relaxation times from creep and stress relaxation (SR) processes as functions of reciprocal temperature. The dashed lines are the VFT curves. Inset is the result of aligning and overlapping two fast relaxations with the β relaxation.

nihan theory (TNM) and the random first-order transition theory (RFOT) [14], the energy barrier of the quenched glasses is almost independent of temperature, and the temperature dependence of the relaxation time in frozen glasses should follow the simple Arrhenius law. In the RFOT theory, the activated transition allows starting from any initial local state. This means that the apparent activation energy below T_g will be significantly smaller than that above the glass transition. The large apparent activation energy above T_g depends on the temperature dependence of configurational entropy [14]. It has also been found in other glasses that there is no super-Arrhenius behavior in the non-equilibrium state below T_g [63-65]. If we ignore the relaxation time limit caused by aging [63], it is acceptable to relate the slow relaxation process in this study to the α relaxation. In Figure 4, the stress relaxation times τ_{slow} obtained above T_g show a Vogel-Fulcher-Tammann (VFT) relationship with temperature, similar to the α relaxation times τ_α obtained by DMA (the raw data is presented in Figures S11 and S12), indicating that α relaxation drives stress relaxation at high temperatures. It is noteworthy that we examined the stability of fitting parameters at small relaxation fractions in the Supplementary Information (as shown in Figures S4-S6). In the dominant region of β relaxation where $1000/T > 2.8$, the α relaxation constitutes less than 20% of the experimental time. By employing a parameter-fixing approach, we can obtain an upper bound on the relaxation time during stress relaxation, which also accounts for the observed increase in slope near $1000/T = 2.8$. In DMA and static viscoelastic tests, there is a difference between single thermal activation and thermomechanical activation. Stress lowers the activation energy barrier and localizes defect activation. Cooperative atomic motion decreases in the glassy state compared with the supercooled liquid state. Thus, the activation energy for slow relaxation in creep and stress relaxation tests is much lower than that for α relaxation in DMA.

The β and α relaxation processes can be modeled as stretched exponential relaxations in viscoelastic deformation, which fully considers the relaxation time distribution in the relaxation process. Then, the relaxation time distribution during stress relaxation can be extracted using the activation energy spectrum model [34,66]. The change of stress with temperature and time can be expressed as $\Delta\sigma(t) = \int_0^{+\infty} P(E)\theta(E,T,t)\mathrm{d}E$, $P(E)\mathrm{d}E$ represents the overall property change resulting from all activation processes within the energy range from $E \to E + \mathrm{d}E$, $\theta(E,T,t) = 1 - \exp[-\nu_0 t \exp(-E/kT)]$ is the characteristic annealing function, where ν_0 is the Debye frequency 10^{13} s^{-1}. The relaxation time of defects with active energy E is $\tau = t = \exp(-E/kT)/\nu_0$, and the distribution of $\ln\tau$ is $H(\ln\tau) = P(E)\mathrm{d}E/\mathrm{d}\ln t = -\mathrm{d}\sigma(t)/\mathrm{d}\ln t$. Figure 5(a) shows the relaxation time distribution during stress relaxation at different temperatures for La_2-MG. Two peaks appear in the

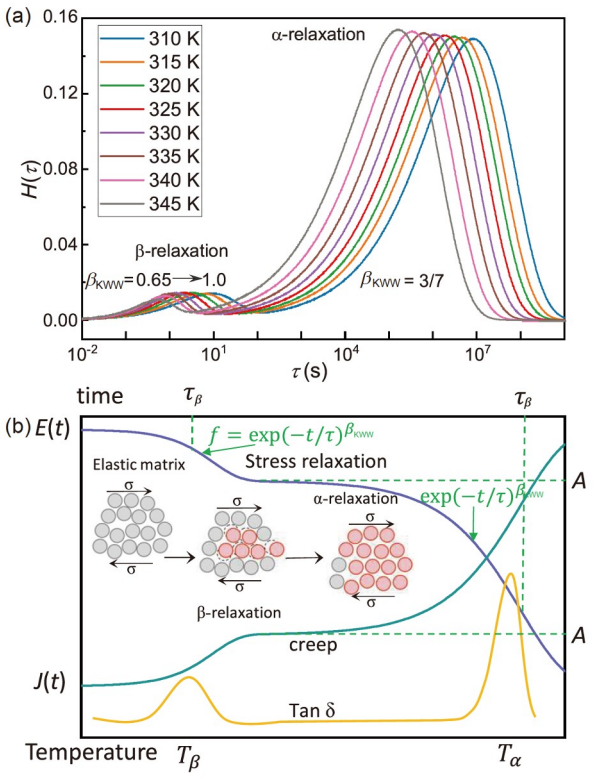

Figure 5 (Color online) (a) The distribution of the relaxation times for the La_2-MG during stress relaxation. The fast portion is considered as β relaxation and the slow one is α relaxation. (b) Schematic illustration of the response of metallic glass external stimuli (strain, stress, temperature). In a very short time, the modulus, compliance, and loss factors remain approximately constant. The system approximates an elastic matrix. With the prolonged influence of temperature or stress, partial atomic motions manifest as β relaxation. At sufficiently long times or very high temperatures, particles undergo large-scale cooperative motion, and α relaxation occurs.

relaxation time spectrum, with a high peak near 10^6 s, which accounts for about 95% of the contribution from α relaxation. The constant stretching exponent β exhibits the same shape on the relaxation spectrum, with the curve shifting leftward as the relaxation time decreases. A small and rather flat peak appears near 10 s, representing the contribution from β relaxation. As the temperature increases, the stretching exponent β increases, and the relaxation peak becomes narrower and shifts leftward. The β relaxation has a typical wideband feature in the frequency domain [67], and the dispersion width increases with decreasing temperature [68,69]. This property indicates that β relaxation comprises a distribution of elementary processes. The β relaxation is generally considered a symmetric distribution process in the frequency domain [68], but in the range of viscoelastic deformation studied in this paper, the contribution of the β relaxation is small. It is then acceptable to use the non-symmetric KWW to approximately describe the β relaxation process. As the temperature increases, β relaxation gradually merges with α relaxation due to its smaller activation energy, and its contribution becomes progressively smaller.

Based on the above analysis, we can establish a physical picture that couples the dynamic relaxation with the viscoelastic deformation. As shown in Figure 5(b), when metallic glass-formers in the glassy state are subjected to external stimuli (strain, stress, temperature), the effects of ballistic motion and cage confinement are neglected since the experimental time scale is much longer than this type of atomic motions, so the system's modulus, compliance, and loss factor remain approximately constant. The system presents itself as a stable elastic matrix. Within the range of 10-100 s or T_β, a subset of atoms in the elastic matrix responds to external stimuli with string-like motions, commonly considered as slow β relaxation [70]. Next, if the experimental temperature is low enough, the modulus or compliance will exhibit a plateau, which represents the transition from β relaxation to α relaxation during the deformation process. Finally, the particles undergo large-scale atomic cooperative motion, which is the α relaxation, at a sufficiently long time or high temperature.

Finally, we would like to discuss the impact of this work on other types of glasses. Similar viscoelastic behavior is commonly observed in polymer glasses [71,72]. In systems with high molecular weight, the relaxation modulus and compliance as a function of time exhibit a rubber plateau, which is believed to be formed by chain entanglement dynamics, showing the transition from the glassy state to the rubber state and then to terminal flow [72]. However, there is no rubber plateau in systems with low molecular weight. Coincidentally, low molecular weight systems often exhibit less pronounced secondary relaxation processes, which is consistent with the findings in this paper. Therefore, it is reasonable to explore a connection between dynamic relaxation and viscoelasticity between metallic and polymeric glasses.

5 Conclusion

In summary, our study highlights a close correlation between dynamic relaxation and viscoelastic deformation. In the stress relaxation and creep processes of MGs, the presence of β relaxation leads to the occurrence of a two-step relaxation process. Both relaxation processes follow the Arrhenius relationship, corresponding respectively to β and α relaxations. Model analysis reveals that the rapid process associated with β relaxation undergoes a transition from a stretched exponential relaxation to a simple Debye relaxation, while the slow relaxation maintains a consistent profile. The insights gained from this research hold significant implications for the design and development of novel glasses with tailored viscoelastic properties.

This work was supported by the National Natural Science Foundation of China (Grant Nos. 51971178, and 52271153), the Natural Science Basic Research Plan for Distinguished Young Scholars in Shaanxi Province (Grant No. 2021JC-12), the Fundamental Research Funds for the Central Universities (Grant No. D5000220034). Yun-Jiang Wang acknowledges the support from the National Natural Science Foundation of China (Grant No. 12072344). Eloi Pineda acknowledges the support from the research project PID2020-112975GB-I00 funded by MCIN/AEI/10.13039/501100011033 and from Generalitat de Catalunya, AGAUR (Grant No. 2021SGR00343). Si Lan acknowledges the partial support from the Natural Science Foundation of China (Grant No. 52222104).

Conflict of interest The authors declare that they have no conflict of interest.

Supporting Information

The supporting information is available online at http://phys.scichina.com and https://link.springer.com. The supporting materials are published as submitted, without typesetting or editing. The responsibility for scientific accuracy and content remains entirely with the authors.

1 K. L. Ngai, *Relaxation and Diffusion in Complex Systems* (Springer, New York, 2011).
2 P. G. Debenedetti, and F. H. Stillinger, Nature **410**, 259 (2001).
3 T. Vogt, and T. Shinbrot, Phys. Rev. Appl. **3**, 050001 (2015).
4 W. Kauzmann, Chem. Rev. **43**, 219 (1948).
5 P. Luo, P. Wen, H. Y. Bai, B. Ruta, and W. H. Wang, Phys. Rev. Lett. **118**, 225901 (2017).
6 C. A. Angell, K. L. Ngai, G. B. McKenna, P. F. McMillan, and S. W. Martin, J. Appl. Phys. **88**, 3113 (2000).
7 J. C. Qiao, Q. Wang, J. M. Pelletier, H. Kato, R. Casalini, D. Crespo, E. Pineda, Y. Yao, and Y. Yang, Prog. Mater. Sci. **104**, 250 (2019).
8 M. D. Ediger, Annu. Rev. Phys. Chem. **51**, 99 (2000).
9 W. H. Wang, Prog. Mater. Sci. **106**, 100561 (2019).
10 M. Jiang, Sci. China-Phys. Mech. Astron. **63**, 106131 (2020).
11 F. H. Stillinger, and P. G. Debenedetti, Annu. Rev. Condens. Matter Phys. **4**, 263 (2013).
12 G. P. Johari, J. Chem. Phys. **58**, 1766 (2003).
13 G. P. Johari, and M. Goldstein, J. Chem. Phys. **53**, 2372 (2003).

14 V. Lubchenko, and P. G. Wolynes, Annu. Rev. Phys. Chem. **58**, 235 (2007).
15 L. M. C. Janssen, Front. Phys. **6**, 97 (2018).
16 Y. Chen, Z. Ye, K. Wang, J. Huang, H. Tong, Y. Jin, K. Chen, H. Tanaka, and P. Tan, Nat. Phys. **19**, 969 (2023).
17 F. Zhu, H. K. Nguyen, S. X. Song, D. P. B. Aji, A. Hirata, H. Wang, K. Nakajima, and M. W. Chen, Nat. Commun. **7**, 11516 (2016).
18 L. Hu, and Y. Yue, J. Phys. Chem. C **113**, 15001 (2009).
19 W. Chu, Z. Wang, N. Ren, B. Dong, J. Yu, P. Guan, Y. Liu, Y. Yue, and L. Hu, Sci. China-Phys. Mech. Astron. **66**, 246112 (2023).
20 X. Monnier, S. Marina, X. Lopez de Pariza, H. Sardón, J. Martin, and D. Cangialosi, Polymers **13**, 954 (2021).
21 D. Cangialosi, V. M. Boucher, A. Alegría, and J. Colmenero, Phys. Rev. Lett. **111**, 095701 (2013).
22 X. Monnier, D. Cangialosi, B. Ruta, R. Busch, and I. Gallino, Sci. Adv. **6**, eaay1454 (2020).
23 W. Bing, X. Q. Gao, and J. C. Qiao, Rare Met. Mater. Eng. **53**, 70 (2024).
24 Y. J. Duan, M. Nabahat, Y. Tong, L. Ortiz-Membrado, E. Jiménez-Piqué, K. Zhao, Y. J. Wang, Y. Yang, T. Wada, H. Kato, J. M. Pelletier, J. C. Qiao, and E. Pineda, Phys. Rev. Lett. **132**, 056101 (2024).
25 F. Spaepen, Acta Metall. **25**, 407 (1977).
26 A. S. Argon, Acta Metall. **27**, 47 (1979).
27 R. Rinaldi, R. Gaertner, L. Chazeau, and C. Gauthier, Int. J. Non-Linear Mech. **46**, 496 (2011).
28 M. D. Demetriou, J. S. Harmon, M. Tao, G. Duan, K. Samwer, and W. L. Johnson, Phys. Rev. Lett. **97**, 065502 (2006).
29 Z. Wang, and W. H. Wang, Natl. Sci. Rev. **6**, 304 (2019).
30 D. Pan, A. Inoue, T. Sakurai, and M. W. Chen, Proc. Natl. Acad. Sci. USA **105**, 14769 (2008).
31 J. S. Harmon, M. D. Demetriou, W. L. Johnson, and K. Samwer, Phys. Rev. Lett. **99**, 135502 (2007).
32 H. B. Yu, W. H. Wang, H. Y. Bai, Y. Wu, and M. W. Chen, Phys. Rev. B **81**, 220201 (2010).
33 Z. Wang, B. A. Sun, H. Y. Bai, and W. H. Wang, Nat. Commun. **5**, 5823 (2014).
34 B. Sun, W. Cao, Z. Wang, B. Sun, and W. Wang, Phys. Rev. B **105**, 014110 (2022).
35 Y. J. Duan, L. T. Zhang, J. C. Qiao, Y. J. Wang, Y. Yang, T. Wada, H. Kato, J. M. Pelletier, E. Pineda, and D. Crespo, Phys. Rev. Lett. **129**, 175501 (2022).
36 Q. Hao, E. Pineda, Y. J. Wang, Y. Yang, and J. C. Qiao, Phys. Rev. B **108**, 024101 (2023).
37 S. Y. Liang, L. T. Zhang, B. Wang, Y. J. Wang, E. Pineda, and J. C. Qiao, Intermetallics **164**, 108115 (2024).
38 L. T. Zhang, Y. J. Duan, D. Crespo, E. Pineda, Y. J. Wang, J. M. Pelletier, and J. C. Qiao, Sci. China-Phys. Mech. Astron. **64**, 296111 (2021).
39 L. Zhang, Y. Wang, Y. Yang, and J. Qiao, Sci. China-Phys. Mech. Astron. **66**, 286111 (2023).
40 W. Jiang, and B. Zhang, J. Appl. Phys. **127**, 115104 (2020).
41 Z. Wang, H. B. Yu, P. Wen, H. Y. Bai, and W. H. Wang, J. Phys.-Condens. Matter **23**, 142202 (2011).
42 N. Nishiyama, K. Takenaka, H. Miura, N. Saidoh, Y. Zeng, and A. Inoue, Intermetallics **30**, 19 (2012).
43 Q. K. Jiang, X. P. Nie, Y. G. Li, Y. Jin, Z. Y. Chang, X. M. Huang, and J. Z. Jiang, J. Alloys Compd. **443**, 191 (2007).
44 W. Kob, and J. L. Barrat, Phys. Rev. Lett. **78**, 4581 (1997).
45 P. Ballesta, A. Duri, and L. Cipelletti, Nat. Phys. **4**, 550 (2008).
46 N. Petzold, and E. A. Rössler, J. Chem. Phys. **133**, 124512 (2010).
47 S. P. Das, Rev. Mod. Phys. **76**, 785 (2004).
48 R. C. Welch, J. R. Smith, M. Potuzak, X. Guo, B. F. Bowden, T. J. Kiczenski, D. C. Allan, E. A. King, A. J. Ellison, and J. C. Mauro, Phys. Rev. Lett. **110**, 265901 (2013).
49 A. Arbe, J. Colmenero, M. Monkenbusch, and D. Richter, Phys. Rev. Lett. **81**, 590 (1998).
50 J. C. Phillips, Rep. Prog. Phys. **59**, 1133 (1996).
51 Y. Yu, M. Wang, D. Zhang, B. Wang, G. Sant, and M. Bauchy, Phys. Rev. Lett. **115**, 165901 (2015).
52 Y. T. Sun, R. Zhao, D. W. Ding, Y. H. Liu, H. Y. Bai, M. Z. Li, and W. H. Wang, Nat. Commun. **14**, 540 (2023).
53 F. Zhu, G. H. Xing, G. J. Lyu, L. T. Zhang, Y. J. Wang, Y. Yang, J. M. Pelletier, and J. C. Qiao, Int. J. Plast. **164**, 103588 (2023).
54 E. E. Ferrero, K. Martens, and J. L. Barrat, Phys. Rev. Lett. **113**, 248301 (2014).
55 B. Ruta, Y. Chushkin, G. Monaco, L. Cipelletti, E. Pineda, P. Bruna, V. M. Giordano, and M. Gonzalez-Silveira, Phys. Rev. Lett. **109**, 165701 (2012).
56 Z. Evenson, B. Ruta, S. Hechler, M. Stolpe, E. Pineda, I. Gallino, and R. Busch, Phys. Rev. Lett. **115**, 175701 (2015).
57 P. Luo, M. X. Li, H. Y. Jiang, R. Zhao, F. Zontone, Q. S. Zeng, H. Y. Bai, B. Ruta, and W. H. Wang, Phys. Rev. B **102**, 054108 (2020).
58 A. I. Taub, Acta Metall. **28**, 633 (1980).
59 A. I. Taub, and F. Spaepen, J. Mater. Sci. **16**, 3087 (1981).
60 G. Ding, F. Jiang, X. Song, L. H. Dai, and M. Q. Jiang, Sci. China-Phys. Mech. Astron. **65**, 264613 (2022).
61 P. Luo, Y. Zhai, P. Falus, V. García Sakai, M. Hartl, M. Kofu, K. Nakajima, A. Faraone, and Y. Z, Nat. Commun. **13**, 2092 (2022).
62 H. Yuan, J. Yan, P. Gao, S. K. Kumar, and O. K. C. Tsui, Sci. Adv. **8**, eabq5295 (2022).
63 J. Zhao, S. L. Simon, and G. B. McKenna, Nat. Commun. **4**, 1783 (2013).
64 V. V. Ginzburg, Soft Matter **16**, 810 (2020).
65 G. B. McKenna, and J. Zhao, J. Non-Crystal. Solids **407**, 3 (2015).
66 M. R. J. Gibbs, J. E. Evetts, and J. A. Leake, J. Mater. Sci. **18**, 278 (1983).
67 Y. B. Yang, Q. Yang, D. Wei, L. H. Dai, H. B. Yu, and Y. J. Wang, Phys. Rev. B **102**, 174103 (2020).
68 K. L. Ngai, S. Capaccioli, M. Paluch, and L. Wang, Philos. Mag. **100**, 2596 (2020).
69 B. Wang, Z. Y. Zhou, P. F. Guan, H. B. Yu, W. H. Wang, and K. L. Ngai, Phys. Rev. B **102**, 094205 (2020).
70 H. B. Yu, R. Richert, and K. Samwer, Sci. Adv. **3**, e1701577 (2017).
71 C. B. Roth, Ed., *Handbook of Chemistry and Physics* (CRC Press, Boca Raton, 2017).
72 G. B. McKenna, and S. L. Simon, Macromolecules **50**, 6333 (2017).